

## UPDATES OF 'AW3D30' ALOS GLOBAL DIGITAL SURFACE MODEL WITH OTHER OPEN ACCESS DATASETS

Junichi Takaku<sup>1,\*</sup>, Takeo Tadono<sup>2</sup>, Masanori Doutsu<sup>1</sup>, Fumi Ohgushi<sup>1</sup>, and Hiroki Kai<sup>1</sup>

<sup>1</sup> Remote Sensing Technology Center of Japan, Tokyu REIT Toranomon BLDG 3F, 3-17-1 Minato-ku Tokyo, Japan –  
(takaku, fumi\_og, dotsu\_masanori)@restec.or.jp

<sup>2</sup> Earth Observation Research Center, Japan Aerospace Exploration Agency, 2-1-1 Sengen, Tsukuba, Ibaraki, Japan –  
tadono.takeo@jaxa.jp

Commission IV, WG IV/3

**KEY WORDS:** Three-Line, Stereoscopic, Satellite, Optical, High resolution, DEM/DTM

### ABSTRACT:

In 2016 we first completed the global data processing of digital surface models (DSMs) by using the whole archives of stereo imageries derived from the Panchromatic Remote sensing Instrument for Stereo Mapping (PRISM) onboard the Advanced Land Observing Satellite (ALOS). The dataset was freely released to the public in 30 m grid spacing as the 'ALOS World 3D - 30m (AW3D30)', which was generated from its original version processed in 5 m or 2.5 m grid spacing. The dataset has been updated since then to improve the absolute/relative height accuracies with additional calibrations. However the most significant update that should be applied for improving the data usability is the filling of void areas, which correspond to approx. 10% of global coverage, mostly due to cloud covers. In this paper we introduce the updates of AW3D30 filling the voids with other open-access DSMs such as Shuttle Radar Topography Mission (SRTM) Digital Elevation Model (DEM), Advanced Spaceborne Thermal Emission and Reflection Radiometer Global DEM (ASTER GDEM), ArcticDEM, etc., through inter-comparisons among these datasets.

### 1. INTRODUCTION

The elevation map of terrain is fundamental data for many geoscience applications e.g., ortho-photo processing, infrastructure design, disaster monitoring, environment monitoring, natural resources survey, and so on. In 2016 we first completed the global data processing of digital surface models (DSMs) by using the whole archives of stereo imageries derived from the Panchromatic Remote sensing Instrument for Stereo Mapping (PRISM) onboard the Advanced Land Observing Satellite (ALOS) (Takaku et al., 2016). The software was exclusively developed for the full-automatic operation of mass data processing based on a traditional optical photogrammetry. The dataset was named 'ALOS World 3D (AW3D)', and has 5 m or 2.5 m grid spacing utilizing the optical triplet stereo imageries in 2.5 m resolution while its accuracy was confirmed at 5 m (rms) in vertical and also 5 m (rms) in horizontal. Its low resolution version of 1 arc-sec (approx. 30 m on the equator) grid spacing (i.e., AW3D30) was then generated from the original version and was freely released to the public (Tadono et al., 2016). The dataset has been updated since then to improve the absolute/relative height accuracies with additional calibrations (Takaku et al., 2017, Takaku et al., 2018). However the most significant update that should be applied for improving usability of the data is the filling of void areas, which correspond to approx. 10 % of global land coverage, mostly due to cloud or snow/ice covers in source PRISM imageries. Figure 1 shows the global coverage of the AW3D30 which consists of total 24,430 1°x1° tiles. The void areas are mainly distributed in the equator zone and high-latitude zones due to the heavy cloud coverage on the tropical

rainforest areas and the snow/ice on the polar areas respectively, as well as in some parts of northern Africa due to the large desert. We decided to generate the void-fill version of the AW3D30 by using the other open-access digital elevation models (DEMs) through inter-comparisons among these different datasets. The process includes some quality updates with detecting / filtering of noise in the original data. In this paper we report on the details of the void-filling process for the AW3D30.

### 2. INPUT DEM DATASETS

The Shuttle Radar Topography Mission (SRTM) DEM 1 arc-sec version 3 (SRTM-1 ver.3) (Rodriguez et al., 2006) was mainly used in the void-filling. The SRTM DEM was generated from the interferometric processing of C-band radar onboard the space shuttle in 2000, covering land areas between N60° and S56° with 1 arc-sec grid spacing. The original SRTM DEM also includes some void areas especially in steep mountainous region; they were filled with Advanced Spaceborne Thermal Emission and Reflection Radiometer Global DEM Version 2 (ASTER GDEM ver.2) (Tachikawa et al., 2011) and Global Multi-resolution Terrain Elevation Data 2010 (GMTED 2010) in the SRTM-1 ver.3.

The Geospatial Information Authority of Japan (GSI) 10 m mesh DEM (GSI10m) (Tachikawa et al., 2011) was used only in Japan instead of the SRTM. The GSI10m is digital terrain models (DTMs) in 0.4 arc-sec (approx. 10 m) grid spacing derived from contour lines of 1/25,000 maps created by the traditional aerial photogrammetry, covering whole land areas in Japan.

\* Corresponding author

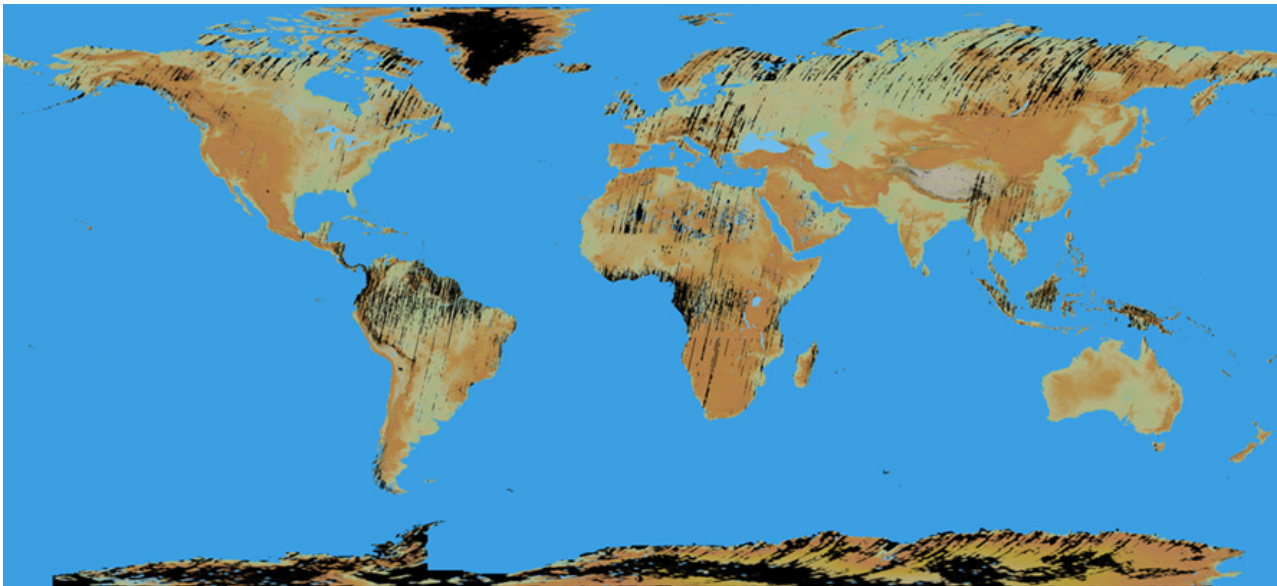


Figure 1. Global coverage of the original AW3D30. Black areas correspond to the voids.

The ArcticDEM (Porter et al., 2018) was used for filling the voids in areas north of  $N60^\circ$  and in some other areas of northern high latitudes i.e., Alaska Peninsula, Aleutian Islands and Kamchatka Peninsula. The data were derived from in-track and cross-track optical stereo imageries of high-resolution ( $\sim 0.5$  m) commercial satellites i.e., WorldView series and GeoEye-1. The dataset covers all land area north of  $60^\circ N$ ; however it also includes some void areas. We used the both of the version 2 mosaic, which has the grid spacing of 5 m, and the latest version 3 mosaic, which has the grid spacing of 2 m, for the void-filling after their inter-comparison with other datasets.

The ASTER GDEM ver.3 (NASA et al., 2019), which was released in 2019 with some quality updates from the GDEM ver.2, was used in the north polar areas and in some other low-middle latitudes where the quality of SRTM-1 ver.3 was relatively low. The data were generated from the along-track optical stereo imageries of 15 m resolution, covering land areas between  $N83^\circ$  and  $S83^\circ$  with 1 arc-sec grid spacing.

The TerraSAR-X add-on for Digital Elevation Measurement (TanDEM-X) 90m DEM (Wessel et al., 2018) was used especially in north polar areas as well. The data were generated from the interferometric processing of X-band bistatic radar onboard the twin satellites flying in close formation, covering all global land areas from pole to pole. It has the grid spacing of 3 arc-secs (approx. 90 m on the equator) as the low-resolution version of the original data which has 0.4 arc-sec grid spacing.

In south of  $56^\circ S$  including Antarctica we have a plan to use Reference Elevation Model of Antarctica (REMA) DSM (Howat et al., 2019) as well as the TanDEM-X 90m DEM and the ASTER GDEM for filling the large void areas, though the data are still in our preliminary validation.

Other than the existing DEM datasets mentioned above we optionally generated additional DSMs from PRISM imageries that have over 30 % cloud covers for the void-filling while the original AW3D was generated only from the imageries that have less than 30 % cloud covers.

### 3. DEM INTER-COMPARISON

The inter-comparison among different datasets was performed for north polar areas where any of the ArcticDEM, the GDEM ver.3, or the TanDEM-X (TDX) 90m DEM is available. We

used two  $1^\circ \times 1^\circ$  tile areas for the comparison:  $N65^\circ W018$  in Iceland and  $N78^\circ W069$  in Greenland. Both tiles include various types of terrain in a height range of approx. 0 ~ 1700 m, while the southern half of  $N78^\circ W069$  is covered by large ice-sheets. Figure 2 and 3 show the comparisons of height maps in shaded-relief with void masks among the AW3D30, the GDEM ver.3, the ArcticDEM ver.3 and the TDX 90m DEM for the tiles of  $N65^\circ W018$  and  $N78^\circ W069$  respectively. In the tile of  $N65^\circ W018$  there are void areas in both of the AW3D30 and the ArcticDEM ver.3, whereas there are no voids in other two datasets.

In the inter-comparison the ArcticDEM and the TDX 90m DEM are down-sampled and up-sampled respectively into 1 arc-sec geodetic latitude-longitude frame of AW3D30, while the GDEM is resampled into the same frame compensating the shift of half pixels derived from the difference of grid definitions between the GDEM and the AW3D30. The WGS84 ellipsoidal heights of the ArcticDEM and the TDX 90m DEM are converted to EGM96 orthometric heights of other two datasets. The relative height difference from the AW3D30 is calculated in each of other three datasets.

Figure 4 and 5 show the height difference images and their histograms of 1 m interval respectively in the two tile areas, while Table 1 and 2 show their statistics. In both tiles there are negative average errors for all compared DSMs, which mean that the heights of AW3D30 are higher than others. They are -23 m to -7 m in the GDEM ver.3, and are -3 m to -2 m in other two datasets. From Fig. 4 it is confirmed that there are some large error segments in the GDEM ver.3 especially at the southern parts of both tiles. In the tile of  $N65^\circ W018$  the errors mostly exceed -100 m and cause the standard deviation of 39 m in Table 1. In the tile of  $N78^\circ W069$  the errors in the southern part are positive with some systematic patterns that may be derived from some processing noise, e.g., filtering of original artifacts. This is reflected to the standard deviation of 14 m in Table 2 as well. In the TDX 90m DEM systematic errors along with original terrain are observed in Fig. 4; these are considered to be derived from the difference of the grid spacing and are reflected to the difference of standard deviations between 9 m and 4 m in Table 1 and 2 respectively because the tile  $N65^\circ W018$  includes steeper terrain. In the tile of  $N78^\circ W069$  the negative errors of TDX 90m DEM in the southern part are relatively larger than the ones of ArcticDEM ver.3, and are

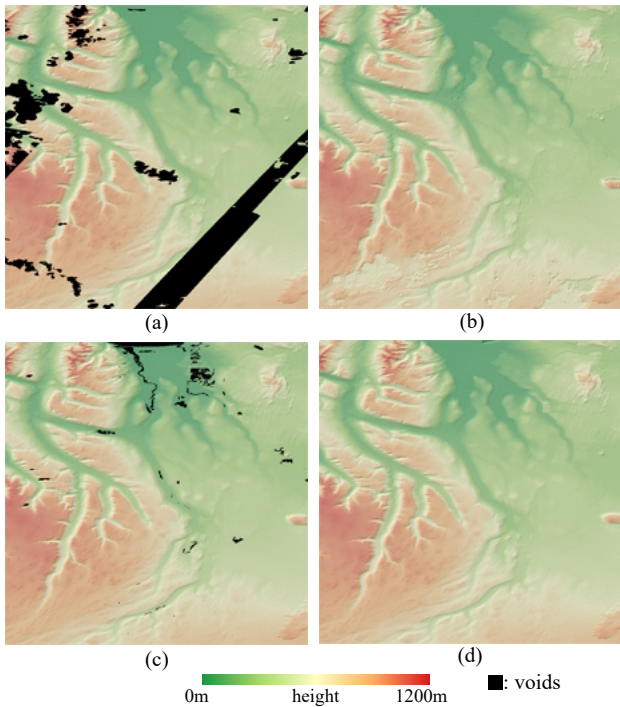


Figure 2. Comparison of DSMs in N65W018.  
(a) AW3D30, (b) ASTER GDEM ver.3,  
(c) ArcticDEM ver.3, (d) TDX 90m DEM.

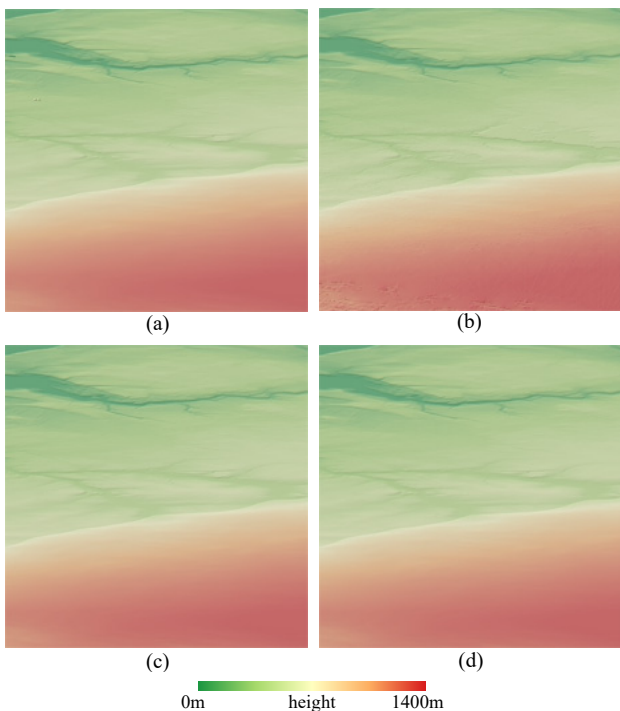


Figure 3. Comparison of DSMs in N78W069.  
(a) AW3D30, (b) ASTER GDEM ver.3,  
(c) ArcticDEM ver.3, (d) TDX 90m DEM.

reflected to the two peaks (-1 m and -6 m) of the histogram in Fig. 5 (b). The difference of errors may possibly be caused by the temporal changes among the acquisitions of source data in the compared DSMs on the large ice-sheets. The penetration of X-band radar signal on the ice-sheets may be another possible cause of the difference (Abdullahi et al., 2019). The ArcticDEM ver.3 has smallest relative height errors from the AW3D30,

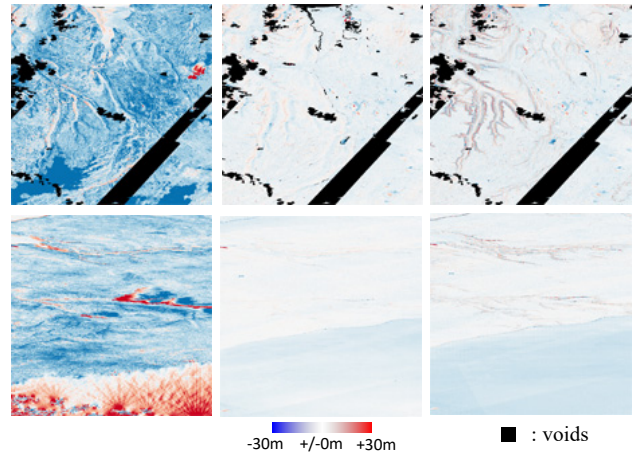


Figure 4. Height differences from AW3D30.  
Top: N65W018, Bottom: N78W069, Left to right: ASTER  
GDEM ver.3, ArcticDEM ver.3, TDX 90m DEM.

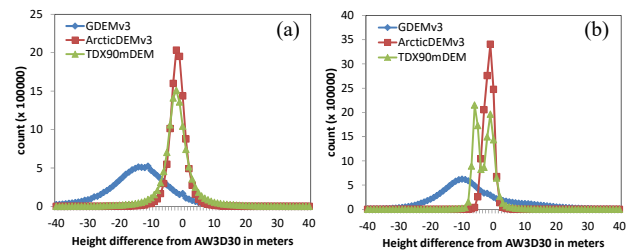


Figure 5. Histograms of height differences from  
AW3D30. (a) N65W018, (b) N78W069

datasets	No. of grids	ave.[m]	std.dev.[m]	max.[m]	min.[m]
ASTER GDEM v3	11650333	-23.04	39.40	198	-825
ArcticDEM v3	11490632	-1.64	4.90	249	-809
TDX 90m DEM	11650333	-1.94	9.05	213	-808

Table 1. Statistics of height differences in N65W018.

datasets	No. of grids	ave.[m]	std.dev.[m]	max.[m]	min.[m]
ASTER GDEM v3	12960000	-6.52	14.32	294	-460
ArcticDEM v3	12960000	-1.52	3.24	257	-455
TDX 90m DEM	12960000	-2.92	4.35	253	-456

Table 2. Statistics of height differences in N78W069.

which the standard deviations are approx. 5 m and 3 m in the two tile areas, though there are some void areas.

As the result we decided to use the ArcticDEM ver.3 as the first priority for the void-filling in north polar areas. The ArcticDEM ver. 2 is used as the second priority in areas where the ver. 3 is void. For the third priority we use the ASTER GDEM ver.3, while the TDX 90m DEM is used as the fourth, considering the consistency of the original grid spacing and of the error trends on the ice-sheets, though it includes large error segments in some areas; they are manually checked and are excluded in the void-filling process.

#### 4. SEA MASK CORRECTION

The sea areas in the AW3D are originally masked by using the existing global water-body-data in public domain i.e., SRTM Water Body Data (SWBD) (NASA/NGA, 2003) or Global Self-consistent, Hierarchical, High-resolution Shoreline Database (GSHHS) (Wessel et al., 1996). However we found some

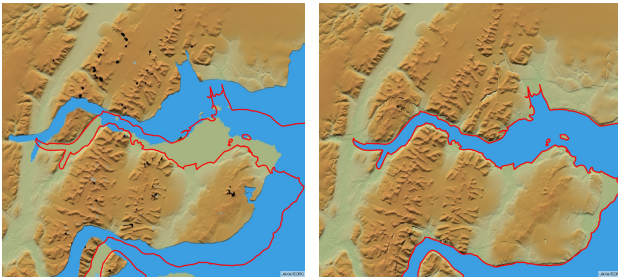


Figure 6. AW3D30 N80W016-021. Left: original, Right: sea masks corrected. Red lines and blue areas depict OSM coastlines and sea masks respectively.

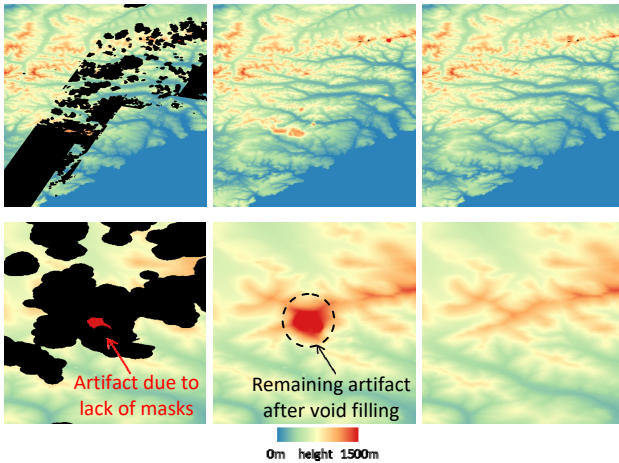


Figure 7. Comparison of AW3D30 DSMs for tile N61E161. Left to right: the original, the void-filled without the filtering, and the one with the filtering. Top: whole tile areas, Bottom: Zoom in an artifact.

inconsistencies between the original sea masks and the PRISM imagery especially in the areas north of  $N60^\circ$  where the GSHHS is used. We conducted a preliminary comparison among some coastline datasets in public domain and decided to replace the SWBD or the GSHHS to OpenStreetMap (OSM) coastlines (OpenStreetMap contributors, 2019) in selected areas through manual inspections. The coastlines in Japanese national base-map released by GSI are used only in Japan instead of the OSM. The additional voids that were derived from the change of the coastlines are filled in the void-filling process as well. Figure 6 shows a sample area of the AW3D30 DSM where the coastline errors of GSHHS are corrected with the OSM

## 5. VOID FILLING WITH FILTERING

For the void-filling we applied the method of “delta surface fill” (DSF) (Grohman et al., 2006) which fills the voids with smoothing the height gaps at boundaries between the original and the filling data without any change in the original data. In the preliminary operation of the void-filling, we detected many obvious artifacts in the AW3D30 especially on areas around voids in the north polar areas. Those errors are due to lack of the cloud/snow masks which were automatically applied scene by scene. The error trends have strong correlation with the number of scene-stacks because the large errors can be discarded in the scene-mosaicking process with a majority rule even if the masks are missed in some scenes. Therefore we applied a filtering process to detect the errors using the

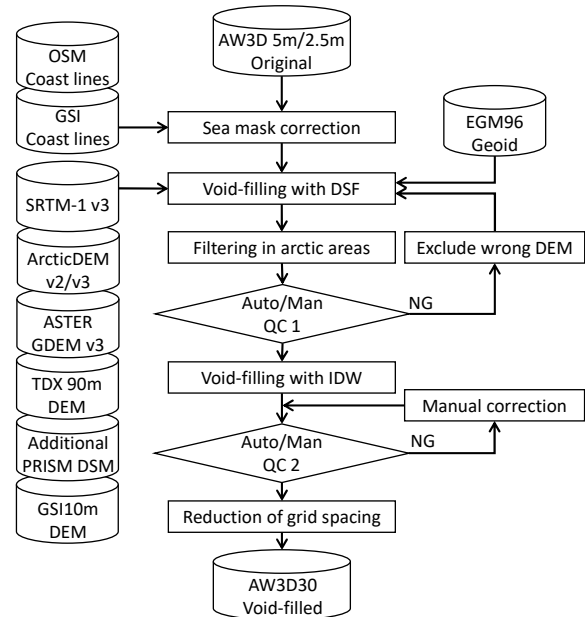


Figure 8. Processing flow of the AW3D void-filling.

ArcticDEM under an assumption that the ArcticDEM has better qualities than the AW3D30 in the areas adjacent to its cloud/snow masks. Namely, the valid data grids that satisfy following conditions are regarded as errors due to lack of masks and are replaced with ArcticDEM:

- ArcticDEM is valid
- Minimum grid distance from the void grids  $\leq T1$
- Number of scene-stacks  $\leq T2$
- Absolute height difference from ArcticDEM  $> T3$
- Grid distance from the grids satisfying d)  $\leq T4$

The condition b) means the adjacent level from the void, while the condition e) means the spatial local margin of height error grids. We determined the thresholds  $T1$ ,  $T2$ ,  $T3$ , and  $T4$  to 200 grids, 2 stacks, 200 m, and 10 grids, respectively, from the preliminary experiments with sample tiles which have various conditions of terrain/voids. Figure 7 shows the comparison of DSMs in a sample  $1^\circ \times 1^\circ$  tile of N61E161 among the original AW3D30, and its void-filled ones by ArcticDEM without and with the filtering. In Fig. 7 the obvious artifacts distributed around the void areas were successfully eliminated with the filtering process.

Figure 8 shows the flow of the void-filling process. It is applied to the AW3D original version of 5 m or 2.5 m grid spacing first. The grid spacing is reduced into 1 arc-sec as the AW3D30 products after all filling process are completed. The results of the void-filling with DSF and the filtering are checked tile by tile to detect artifacts in filled areas. If an obvious artifact is detected the filling process will be re-tried after excluding the corresponding external DEM. For the voids remaining after all existing DEMs were applied we optionally use a simple interpolation with the inverse distance weight (IDW) method to fill them depending on the condition of the void e.g., the size, shape, its surrounding terrain, etc. The result of the interpolation is checked manually for each void segment to decide its acceptance.

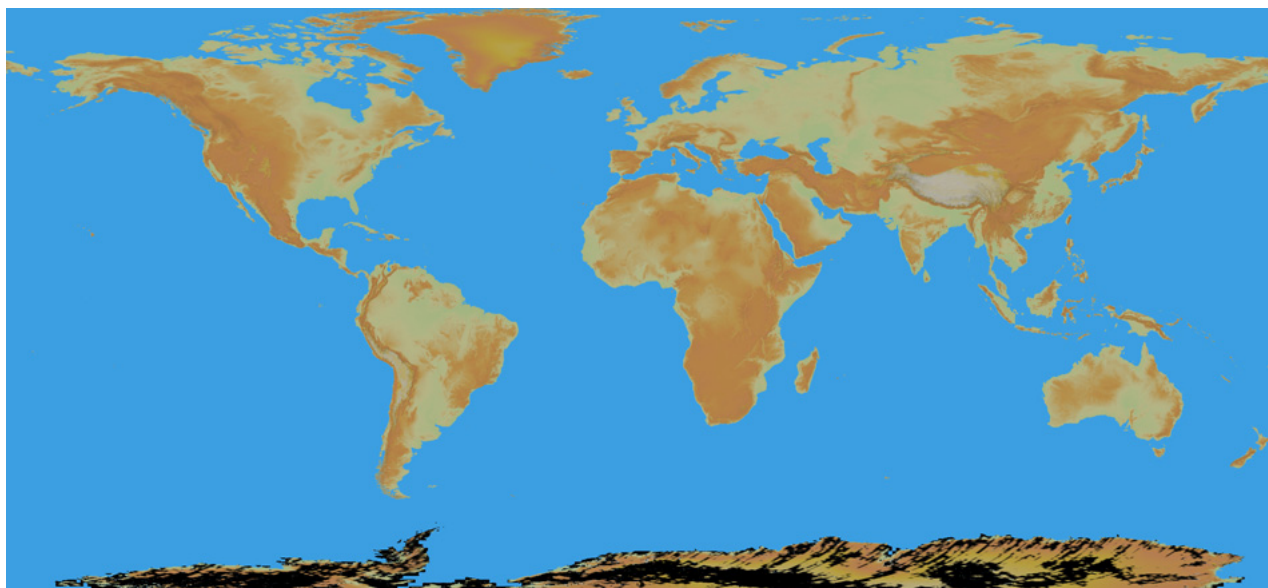


Figure 9. Global coverage of the AW3D30 void-filled version 3.1.

Black areas indicate remaining voids after the filling process. The voids in Antarctica has not been filled as of Mar. 2020.

## 6. RESULTS

The updates for the void-filling of AW3D30 have been executed in stages year by year since the first release in 2016 with the improvements of the height accuracy of the original data. In March 2017 the first update (ver. 1.1) was completed between  $N60^\circ$  and  $S60^\circ$  by filling the voids with the SRTM-1 ver.3 and the GSI10m. In March 2018 the second update (ver. 2.1) was completed by replacing the heights under land-water masks between  $N60^\circ$  and  $S60^\circ$  with the SRTM-1 ver.3 and the GSI10m as well, because we detected large amount of errors in these data that were interpolated from their surrounding valid heights. In March 2019 the third update (ver. 2.2) was completed with filling the voids in north of  $60^\circ N$  with the ArcticDEM ver.2 and the ASTER GDEM ver.2. In March 2020 the latest update (ver. 3.1) was completed by filling or re-filling the voids between  $90^\circ N$  and  $60^\circ S$  with the ArcticDEM ver.3, the ASTER GDEM ver.3, and the TDX 90m DEM.

Figure 9 shows the global coverage of the AW3D30 void-filled ver. 3.1, which the all voids except for Antarctica are filled with external open-access DEMs. The index flags that indicate source datasets used in the void-filling were stored in the ancillary mask files of AW3D30 data products. Table 3 and 4 show the proportions of source data in the AW3D30 ver. 3.1 between  $N60^\circ$  and  $S60^\circ$  (low-middle latitudes) and between  $N90^\circ$  and  $N60^\circ$  (arctic latitudes), respectively. In low-middle latitudes the voids of approx. 10.1 % in original AW3D30 all land areas were mostly filled with SRTM-1 ver.3 with the rate of 9.8 %. The ArcticDEM was used in limited void-areas around  $N60^\circ$  i.e., Alaska Peninsula, Aleutian Islands and Kamchatka Peninsula with the rate of 0.1 %. The GDEM ver.3 was used for voids in high steep mountainous areas where the quality of SRTM-1 ver.3 was not enough i.e., a few tiles in Himalaya and Patagonia, while the TDX 90m DEM was used for a few tiles in Sahara desert. In arctic latitudes the voids of approx. 24.5 % in original AW3D30 all land areas were mostly filled with ArcticDEM ver.3 with the rate of 22.9 %, while a few void areas in both of the AW3D30 and the ArcticDEM ver.3 were filled with the ArcticDEM ver.2. The GDEM ver.3

Source	No. of grids	%
AW3D30 original	135,089,227,573	89.930
SRTM-1 v3	14,758,326,308	9.825
ArcticDEM v3	178,191,652	0.119
ArcticDEM v2	18,831,796	0.013
GDEM v3	121,497,575	0.081
TDX 90m DEM	38,638,832	0.026
PRISM DSM (add.)	3,615,270	0.002
GSI10m (Japan)	5,298,107	0.004
IDW	2,970,655	0.002
total	150,216,597,768	100

Table 3. Proportion of source data in the AW3D30 ver. 3.1 between  $N60^\circ$  and  $S60^\circ$  (low-middle latitudes)

Source	No. of grids	%
AW3D30 original	16,244,112,293	75.476
ArcticDEM v3	4,934,024,291	22.925
ArcticDEM v2	122,249,088	0.568
GDEM v3	184,645,773	0.858
TDX 90m DEM	36,921,800	0.172
PRISM DSM (add.)	3,908	0.000
IDW	231,584	0.001
total	21,522,188,737	100

Table 4. Proportion of source data in the AW3D30 ver. 3.1 between  $N90^\circ$  and  $N60^\circ$  (arctic latitudes)

was used with the rate of 0.9 % in some areas mainly in Fennoscandian Peninsula where relatively large voids are remaining in both of the AW3D30 and the ArcticDEM. The TDX 90m DEM was used in a few areas where the GDEM ver.3 includes large blunders.

The perspective absolute height accuracies of the AW3D30 ver. 3.1 were validated with Ice, Cloud, and land Elevation Satellite (ICESat) data for each of source DEM datasets. The absolute height accuracy of the global spaceborne light-detection-and-ranging (LiDAR) data is less than one meter for the points selected in optimal conditions (Duong et al., 2009). We used the ICESat data products GLA14 in the validation (Zwally et al. 2012). In the calculation of the height difference the 1 arc-sec

Source	N60-S60 (low-middle latitudes)				N90-N60 (arctic latitudes)				N90-S60 (whole except for Antarctica)			
	no. of samples	ave.	std.dev.	rms	no. of samples	ave.	std.dev.	rms	no. of samples	ave.	std.dev.	rms
AW3D30 original	170,542,794	0.04	3.27	3.27	45,666,473	0.52	2.92	2.97	216,209,267	0.14	3.21	3.21
SRTM-1 v3	15,321,801	-0.49	5.04	5.06	-	-	-	-	15,321,801	-0.49	5.04	5.06
ArcticDEM v2	9,471	-4.37	6.97	8.23	269,323	-1.16	5.97	6.08	278,794	-1.27	6.03	6.16
ArcticDEM v3	101,628	-2.21	6.11	6.50	19,333,051	-1.30	3.11	3.38	19,434,679	-1.31	3.14	3.40
GDEM v3	20,414	-0.94	13.23	13.27	305,281	-4.39	8.77	9.81	325,695	-4.17	9.15	10.06
TDX 90m DEM	81,476	-1.39	2.64	2.99	82,815	-0.71	7.37	7.40	164,291	-1.05	5.56	5.66
PRISM DSM (add.)	1,114	-1.59	9.23	9.37	-	-	-	-	1,114	-1.59	9.23	9.37
GSI10m (Japan)	3,268	-2.00	6.06	6.39	-	-	-	-	3,268	-2.00	6.06	6.39
IDW	7,329	-10.22	18.76	21.36	157	-0.42	9.18	9.19	7,486	-10.02	18.66	21.18

Table 5. Statistics of height errors from ICESat GLA14 in AW3D30 void-filled ver. 3.1 (in meters).

(30m) grid data of the AW3D30 under the ICESat's footprint of 70 m in diameter is averaged, while the averaged samples where the standard deviation in the averaging heights exceed 5 m are omitted because the samples in the steep/rough terrain may have less reliability (Huber et al., 2009). After the comparison the samples, where the heights of ICESat were higher in more than 100 m, are associated with outliers due to the cloud reflections or saturated waveforms in ICESat data and are excluded from the results (Carabajal et al. 2006).

Table 5 shows the statistics of height errors from ICESat GLA14 for each of source DEM data in the AW3D30 void-filled ver. 3.1 at the latitudes between N60° and S60° (low-middle latitudes), between N90° and N60° (arctic latitudes), and their composite. Note that the results do not mean the comparison among the accuracies of datasets because the numbers as well as the areas of samples are different among them.

In low-middle latitudes the rms values for both of the AW3D30 original and the TDX 90 m DEM are approx. 3 m, and are enough consistent with their specification accuracy of 5 m (rms) and below 10 m (absolute, LE90) respectively in their original datasets. The rms value for the SRTM-1 ver.3, which was used to fill almost voids in this latitude range, is approx. 5 m and consistent with the specification accuracy of the AW3D original. The rms values of ArcticDEM two versions are approx. 7~8 m; these relatively large values may be derived from their limited distributions in mountainous Islands and Peninsulas around the Bering Sea. The GDEM ver.3 also has large rms of 13 m possibly due to its limited distribution at very high steep mountains in addition to its original accuracy. The additional PRISM DSM has large rms value of 9 m as well; the quality of source imagery which have over 30 % cloud covers, as well as less stacking scenes, may be the cause. The IDW interpolation area has largest errors of 21 m in rms. One possible cause is that the interpolation lost details in some steep terrain though all the results were manually inspected.

In arctic latitudes the rms value of AW3D30 original is almost the same as the one in the low-middle latitudes, while the one of ArcticDEM ver.3, which was used to fill almost voids in this arctic range especially on large ice-sheets in Greenland, is approx. 3 m and is better than the one in the low-middle latitudes. The rms value of the TDX 90m DEM is approx. 7 m and is more than twice as large as the one in low-middle latitudes because the samples in arctic latitudes are distributed in relatively steep terrain, whereas in low-middle latitudes they are distributed mostly in the flat desert. The rms value of the GDEM ver.3 is approx. 10 m where the obvious large blunders were manually excluded in the filling process. The rms of the IDW is 9 m; however it is not enough reliable due to relatively very small number of samples. The global statistics except for

Antarctica, which corresponds to the composition of these two latitude ranges, follow their results.

## 7. CONCLUSION

The updates of AW3D30 global DSM datasets with other open access datasets were presented. The voids in original dataset except for Antarctica, which correspond to approx. 10 % of global land coverage mostly due to cloud or snow/ice covers, were filled with existing open access DEM datasets that were prioritized through inter-comparisons among them. The perspective absolute accuracies of the void filled datasets were validated for each of source datasets with the ICESat global point cloud reference. The result showed that the accuracies of void-filled areas are almost consistent with the areas of AW3D30 original dataset except for some limited areas in extreme terrain.

For future work we have a plan to fill the remaining voids in Antarctica to complete the void-free global DSM datasets until March 2021 by using the REMA DSM, as well as the TDX 90m DEM and the ASTER GDEM. Moreover, we will continue to update the datasets for better quality/accuracy with applying upcoming new datasets including the DSM generated from the cross-track stereo imagery of the ALOS-3, a follow-on satellite of optical sensors onboard the ALOS (Takaku et al., 2019).

## REFERENCES

- Abdullahi, S., Wessel, B., Huber, M., Wendleder, A., Roth, A., Kuenzer, C., 2019. Estimating Penetration-Related X-Band InSAR Elevation Bias: A Study over the Greenland Ice Sheet. *Remote Sens.* 2019, 11, 2903. doi.org/10.3390/rs11242903.
- Carabajal, C., Harding, D., 2006. SRTM C-band and ICESat laser altimetry elevation comparisons as a function of tree cover and relief. *Photogrammetry Engineering and Remote Sensing*, 72(3), pp. 287–298.
- Duong, H., Lindenbergh, R., Pfeifer, N., Vosselman, G., 2009. ICESat Full-Waveform Altimetry Compared to Airborne Laser Scanning Altimetry Over The Netherlands. *IEEE Transaction on Geoscience and Remote Sensing*, 47(10), pp. 3365-3378.
- Grohman, G., Kroenung, G., Strebeck, J., 2006. Filling SRTM voids: The delta surface fill method. *Photogrammetric Engineering and Remote Sensing*, 72 (3), pp. 213-216.
- Howat, I. M., Porter, C., Smith, B. E., Noh, M.-J., Morin, P., 2019. The Reference Elevation Model of Antarctica. *The Cryosphere*, 13, pp. 665-674.

- Huber, M., Wessel, B., Kosmann, D., Felbier, A., Schwieger, V., Habermeyer, M., Wendleder, A., Roth, A., 2009. Ensuring globally the TanDEM-X height accuracy: Analysis of the reference data sets ICESat, SRTM and KGPS-Tracks. *Proc. IEEE IGARSS 2009*, Vol. II, pp.769-772.
- NASA/METI/AIST/Japan Spacesystems, U.S./Japan ASTER Science Team, 2019. ASTER Global Digital Elevation Model V003. NASA EOSDIS Land Processes DAAC. doi.org/10.5067/ASTER/ASTGTM.003. (2019).
- NASA/NGA, 2003. "SRTM Water Body Data Product Specific Guidance". [http://dds.cr.usgs.gov/srtm/version2\\_1/SWBD/SWB\\_D\\_Documentation/SWBD\\_Product\\_Specific\\_Guidance.pdf](http://dds.cr.usgs.gov/srtm/version2_1/SWBD/SWB_D_Documentation/SWBD_Product_Specific_Guidance.pdf). (20 Mar. 2014).
- OpenStreetMap contributors, Planet dump 2019. <https://planet.osm.org>, <https://www.openstreetmap.org>.
- Porter, C., Morin, P., Howat, I., Noh, M.-J., Bates, B., Peterman, K., Keeseey, S., Schlenk, M., Gardiner, J., Tomko, K., Willis, M., Kelleher, C., Cloutier, M., Husby, E., Foga, S., Nakamura, H., Platson, M., Wethington, M., Jr., Williamson, C., Bauer, G., Enos, J., Arnold, G., Kramer, W., Becker, P., Doshi, A., D'Souza, C., Cummens, P., Laurier, F., Bojesen, M., 2018. ArcticDEM. doi.org/10.7910/DVN/OHHUKH, Harvard Dataverse, V1, (15 Jan. 2020).
- Rodriguez, E., Morris, C. S., Belz, J. E., 2006. A Global Assessment of the SRTM Performance. *Photogrammetric Engineering and Remote Sensing*, 72(3), pp.249-260.
- Tachikawa, T., Hato, M., Kaku, M., Iwasaki, A., 2011. Characteristics of ASTER GDEM version 2. *Proc. IEEE IGARSS 2011*, pp. 3657-3660.
- Tadono, T., Nagai, H., Ishida, H., Oda, F., Naito, S., Minakawa, K., Iwamoto, H., 2016. Initial Validation of the 30 m-mesh Global Digital Surface Model Generated by ALOS PRISM. *Int. Arch. Photogramm. Remote Sens. Spatial Inf. Sci.*, XLI-B4, pp.157-162.
- Takaku, J., Tadono T., Tsutsui, K., Ichikawa, M., 2016. Validation of 'AW3D' Global DSM Generated from ALOS PRISM. *ISPRS Ann. Photogramm. Remote Sens. Spatial Inf. Sci.*, III-4, pp. 25-31.
- Takaku, J., and Tadono, T., 2017. Quality updates of 'AW3D' global DSM generated from ALOS PRISM. *Proc. IEEE IGARSS 2017*, pp. 5666-5669.
- Takaku, J., Tadono, T., Tsutsui, K., Ichikawa, M., 2018. Quality Improvements of 'AW3D' Global DSM Derived from ALOS PRISM. *Proc. IEEE IGARSS 2018*, pp. 1612-1615.
- Takaku, J., Tadono, T., Ohgushi, F., Doutsu, M., 2019. High resolution DSM generation from ALOS-3 stereo imageries. *Proc. IEEE IGARSS2019*, pp. 1144-1147.
- Wessel, B., Huber, M., Wohlfart, C., Marschalk, U., Kosmann, D., Roth, A., 2018. Accuracy Assessment of the Global TanDEM-X Digital Elevation Model with GPS Data. *ISPRS Journal of Photogrammetry and Remote Sensing*. Vol. 139, pp. 171-182.
- Wessel, P., Smith, W. H. F., 1996. A Global Self-consistent, Hierarchical, High-resolution Shoreline Database. *Journal of Geophysical Research*, 101(B4), pp. 8741-8743.
- Zwally, H., Schutz, R., Hancock, D., Dimarzio, J., 2012. GLAS/ICESat L2 Global Land Surface Altimetry Data (HDF5). Version 33. NASA DAAC at the National Snow and Ice Data Center, Boulder, CO, USA.